Nanoscale Research Letters

NANO EXPRESS Open Access

Electronic and Magnetic Properties of Defected Monolayer WSe_2 with Vacancies

Danxi Yang, Xiaoli Fan*, Fengxia Zhang, Yan Hu and Zhifen Luo

Abstract

By adopting the first-principle methods based on the density functional theory, we studied the structural, electronic, and magnetic properties of defected monolayer WSe_2 with vacancies and the influences of external strain on the defected configurations. Our calculations show that the two W atom vacancies (V_{W2}) and one W atom and its nearby three pairs of Se atom vacancies (V_{WSe6}) both induce magnetism into monolayer WSe_2 with magnetic moments of 2 and 6 μ_B, respectively. The magnetic moments are mainly contributed by the atoms around the vacancies. Particularly, monolayer WSe_2 with V_{W2} is half-metallic. Additionally, one Se and one W atom vacancies (V_{Se}, V_W), two Se atom vacancies ($V_{Se\text{-}Se}$), and one W atom and the nearby three Se atoms on the same layer vacancy (V_{WSe3})-doped monolayer WSe_2 remain as non-magnetic semiconducting. But the impure electronic states attributed from the W d and Se p orbitals around the vacancies locate around the Fermi level and narrow down the energy gaps. Meanwhile, our calculations indicate that the tensile strain of 0~7% not only manipulates the electronic properties of defected monolayer WSe_2 with vacancies by narrowing down their energy gaps, but also controls the magnetic moments of V_W-, V_{W2}-, and V_{WSe6}-doped monolayer WSe_2.

Keywords: Monolayer WSe_2, Vacancy, External strain, Electronic properties, Magnetic properties, First-principle calculations

Introduction

Unlike gapless graphene [1, 2], semiconducting transition metal dichalcogenide (TMD) monolayers with a band gap of 1~2 eV [3–6] have superior advantages in the fields of catalyst, electronics, and optoelectronics because of their unique chemical, optical, and electronic properties [3–9]. Particularly, monolayer WSe_2 is semiconducting with a direct band gap of ~ 1.6 eV [4, 10–12]. Additionally, its carrier mobility is around 250 cm^2/V, and the on/off ratio is higher than 10^6 at room temperature [13]. More importantly, monolayer WSe_2 is the first TMD showing p-type conducting behavior with high work function metal (Pd) being the contacts [13]. Because of these novel properties, monolayer WSe_2 has been widely studied as the promising candidate in the future electronics and optoelectronics [4, 6, 13–16]. However, monolayer WSe_2 is non-magnetic which limits its application in many other fields related with magnetism.

Based on the previous studies [17–25], structural defects significantly influence the mechanical, electronic, and magnetic properties. For example, point defect and vacancy defect introduce magnetism into graphene [19, 20], MoS_2 monolayer, and $BaTiO_3$(001) thin film [21–23], respectively. Wu et al. studied the effects of defects on the device transmission performance in monolayer WSe_2 tunneling field-effect transistors (TFSTs) by performing the ab initio calculation, which indicates that defects can be well designed to obtain high-performance TFETs [25]. Meanwhile, structural defects were found in the as-grown 2D materials due to the imperfection of the growth process [19, 20, 26–28]. For example, intrinsic structural defects, such as point defects, are noticeable in the as-grown monolayer WSe_2 [26].

Indeed, structural engineering methods including irradiation by high energy particles of electron beam [29], ion beam [30] and high energy laser, and chemical etching [31, 32] are the effective techniques to induce defects in the 2D materials and have been used to modify the atomic structures. Therefore, it is not only significant but also realistic to study the influence of structural defects such

* Correspondence: xlfan@nwpu.edu.cn
State Key Laboratory of Solidification Processing, Centre of Advanced Lubrication and Seal Materials, School of Material Science and Engineering, Northwestern Polytechnical University, 127 YouYi Western Road, Xi'an 710072, Shannxi, China

as vacancies on the properties of monolayer WSe_2, which may offer us the new feature. Additionally, the 2D materials can withstand large strains before rupture and even be stretched beyond the inherent limit of 10% owing to their strong plastic deformation ability as demonstrated on monolayer MoS_2 [33, 34]. Thus, strain engineering has been widely used to tune the properties of 2D materials and enhance the relevant performance in the related applications [11, 17, 33–39]. According to Yang et al.'s study, nanoscale local strain modifies the optical band gap and changes the electronic and magnetic properties of monolayer $ReSe_2$ [38]. Particularly, it was reported that the non-magnetic WS_2 monolayer becomes ferromagnetic under the applied biaxial strain, and the highest magnetic moment reaches 4.85 μ_B [39].

In this work, we systematically investigated the effects of vacancy defects and tensile strain on the electronic properties of monolayer WSe_2. We calculated several vacancy defects of single atom vacancy, double atom vacancy, and big vacancies of four and seven atoms. We found that all the vacancy defects change the electronic properties of monolayer WSe_2, while only the V_{W2} and V_{WSe6} vacancies introduce the magnetism of 2 and 6 μ_B, respectively. Additionally, monolayer WSe_2 with V_W vacancy converts into magnetic from non-magnetic under the external tensile strain. More importantly, the external biaxial strain effectively modulates not only the energy gaps but also the magnetic moments of V_W-, V_{W2}-, and V_{WSe6}-doped monolayer WSe_2. Our calculations suggest defected monolayer WSe_2 with vacancies as potential monolayer magnetic semiconductors.

Computational Methods

All the calculations in the present study were performed by adopting the Vienna Ab initio Simulation Package (VASP) based on density functional theory (DFT) [40, 41]. The Perdew–Burke–Ernzerhof (PBE) method was used to calculate the electronic exchange interaction [42]. The ion–electron and electron–electron interactions were calculated by the projector augmented wave (PAW) method and the plane wave basis set [43, 44]. The cutoff energy for the plane wave basis set was set to 300 eV, and the first Brillouin zone was sampled by the 3 × 3× 1 k-mesh based on the Monkhorst–Pack method [45]. A vacuum space of 15 Å was added along the vertical direction above the monolayer to remove the interactions between the adjacent images in the periodic slab model. Structure relaxations have been carried out until all the forces on each ion are less than 0.02 eV/Å, and the convergence criteria for the total energy were set as 10^{-4} eV. The biaxial tensile strain was imposed on the vacancy defect–doped monolayer WSe_2, which was calculated by $\varepsilon = (c - c_0)/c_0 \times 100\%$, where c and c_0 are the lattice parameters of the strained and free monolayer WSe_2, respectively.

Results and Discussion

Atomic Structure and Electronic Properties of Monolayer WSe_2

The most stable crystal structure of monolayer WSe_2, denoted as 1H-WSe_2, is shown in Fig. 1a, which shows the sandwiched layer of Se-WSe. In 1H-WSe_2, W atoms and Se atoms occupy the sublattices of hexagonal sheet, and the Se atoms on the lower layer are directly underneath

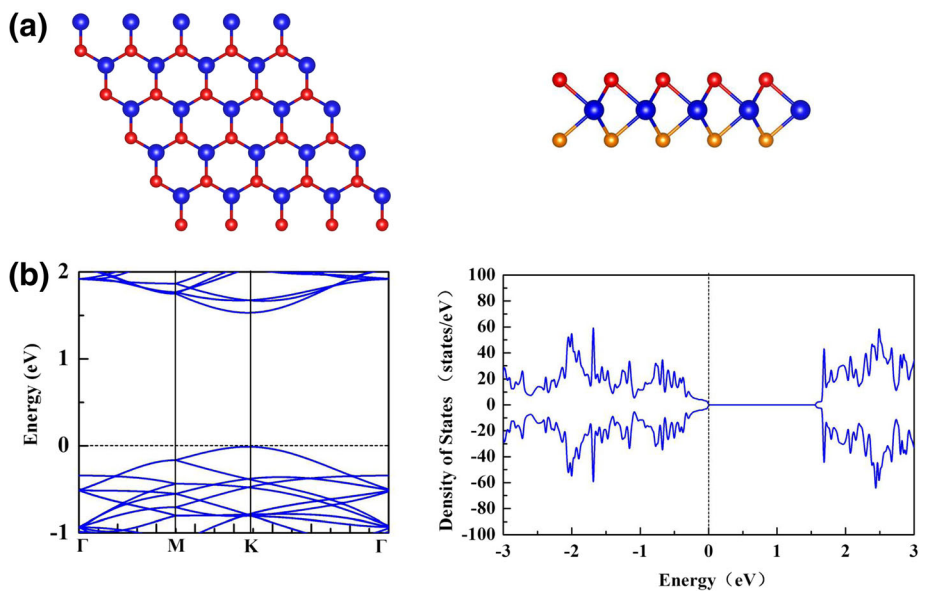

Fig. 1 **a** Top and side views for the atomic structure of monolayer WSe_2. **b** The electronic band structure and density of states (DOS) of monolayer WSe_2. The blue, red, and tangerine balls represent Wand Se atoms on the top and bottom layer, respectively. Fermi level is set as 0 eV

those Se atoms on the upper layer. Our calculated W-W bond length is 3.31 Å and the W-Se bond length is 2.54 Å, agreeing well with previous results [10, 11]. As shown in Fig. 1b, the calculated electronic band structure and density of states (DOS) for 1H-WSe_2 indicate that 1H-WSe_2 is non-magnetic semiconducting with a direct band gap of 1.54 eV. Our calculated result agrees well with the previous result of 1.55 eV [12]. To get a more accurate band gap, we adopted the Heyd–Scuseria–Ernzerh (HSE06) [46] method to calculate the electronic band structure. The energy gap of 1H-WSe_2 calculated by HSE06 method is 2.0 eV.

The Magnetic and Electronic Properties of Defected Monolayer WSe_2 with Vacancy

We considered seven vacancy defect configurations for monolayer WSe_2 in the present study. They are the single atom vacancies including one Se atom vacancy (V_{Se}), one W atom vacancy (V_W), and two atom vacancies of $V_{Se\text{-}Se}$, V_{Se2}, and V_{W2}. The two Se atom vacancy $V_{Se\text{-}Se}$ means the two Se atoms which are just beneath or above each other are removed, while the V_{Se2}/V_{W2} vacancy means that the two adjacent Se/W atoms are removed. We also considered the big vacancies of V_{WSe3} and V_{WSe6}. V_{WSe3} denotes the vacancy of one W atom and the nearby three Se atoms on the same layer, and V_{WSe6} presents the vacancy of one W atom and the nearby three pairs of Se atoms. The optimized structures of monolayer WSe_2 with vacancies of V_{Se}, $V_{Se\text{-}Se}$, V_{Se2}, V_W, V_{W2}, V_{WSe3}, and V_{WSe6} are shown in the insets of Fig. 2. As we can see, the 5 × 5 × 1 supercell was used for the present study of the defected monolayer WSe_2.

Table 1 summarizes the results for the defected monolayer WSe_2 with vacancies of V_{Se}, $V_{Se\text{-}Se}$, V_{Se2}, V_W, V_{W2}, V_{WSe3}, and V_{WSe6}. We can see that the W-W distances around the vacancies of V_{Se}, $V_{Se\text{-}Se}$, and V_{Se2} decrease respectively by 0.23, 0.52, and 0.24 Å compared with the original W-W distance in monolayer WSe_2, which means that the W atoms around the Se atoms vacancies get close to each other. Additionally, the W-W distances around the vacancies of V_W, V_{W2}, and V_{WSe3} slightly increase by 0.02, 0.01, and 0.06 Å. And those W-W distances around the single atom vacancies (V_{Se} /V_W) are almost equal to the counterpart around the two atoms vacancies (V_{Se2}/V_{W2}). For the bigger vacancy V_{WSe6}-doped monolayer WSe_2, the W-W distances between the neighboring W atoms at the corners of the vacancy reduce by 0.58 Å, but the W-W distances at the edges of the vacancy increase by 0.44 Å. The formation energies of the seven vacancy geometries are calculated via:

$$E_{\text{form}} = E_{\text{van-WSe}_2} - E_{\text{WSe}_2} + \Sigma n_i u_i$$

$E_{\text{van-WSe}_2}$ and E_{WSe_2} are the total energies of the 5 × 5 × 1 supercell of monolayer WSe_2 with and without vacancy defect, and u_i and n_i (i = Se, W) are the chemical potential and number of the removed i atom. As listed in Table 1, our calculated formation energies for the seven vacancies indicate that V_{Se}, the single Se atom vacancy, should be frequently observed on WSe_2 monolayer, consistent with the previous result of monolayer MoS_2 [17, 21]. For the two Se atom vacancies of $V_{Se\text{-}Se}$ and V_{Se2}, the formation energy of V_{Se2} is a little higher than that of $V_{Se\text{-}Se}$, indicating that $V_{Se\text{-}Se}$ is energetically

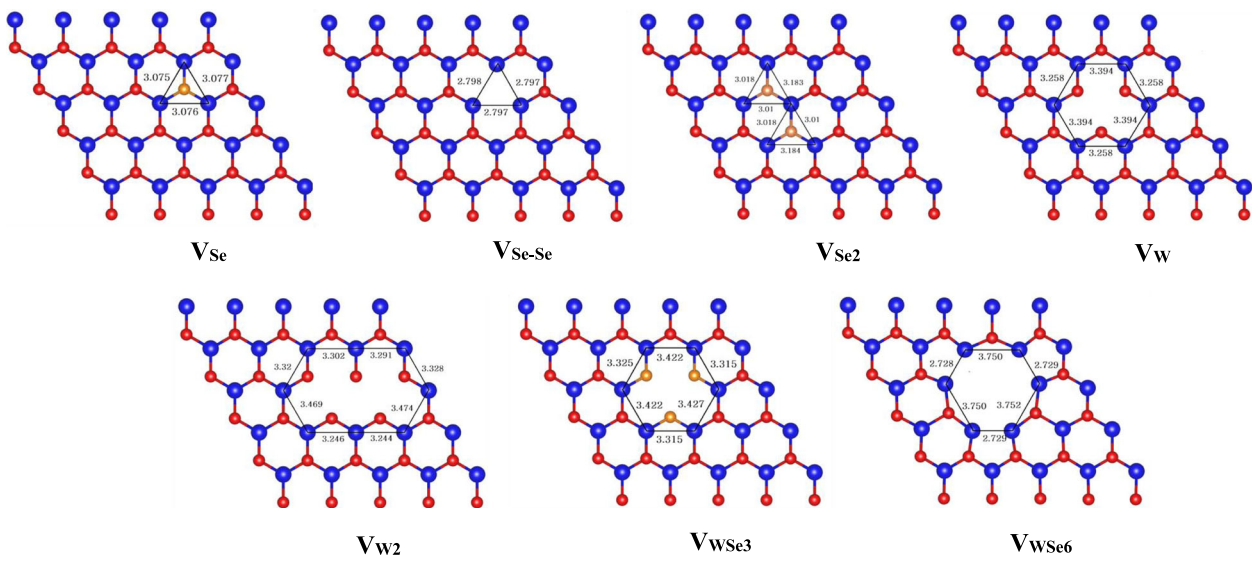

Fig. 2 The optimized atomic structures of monolayer WSe_2 with V_{Se}, $V_{Se\text{-}Se}$, V_{Se2}, V_W, V_{W2}, V_{WSe3}, and V_{WSe6} vacancies. The blue, red, and tangerine balls represent W and Se atoms on the top and bottom layer, respectively

Table 1 The calculation results for monolayer WSe_2 with V_{Se}, $V_{Se\text{-}Se}$, V_{Se2}, V_W, V_{W2}, V_{WSe3}, and V_{WSe6} vacancies

	1H-WSe_2	V_{Se}	V_{Se-Se}	V_{Se2}	V_W	V_{W2}	V_{WSe3}	V_{WSe6}
d_{W-W} (Å)	3.31	3.08	2.79	3.07	3.33	3.32	3.37	2.73[a]/3.75[b]
E_{gap} (eV)	1.54	1.18	1.15	1.02	0.18	0.19 [c]	0.76	0.1
M_{tot} (μ_B)	0	0	0	0	0	2	0	6
E_{form} (eV)	–	2.66	4.7	5.39	5.35	9.43	8.85	16.55

d_{W-W} the averaged W-W distances around the vacancy; E_{gap} and M_{tot} the energy gaps and total magnetic moments, respectively; E_{form} the formation energy. The calculation results for the perfect 1H-WSe_2 are also listed.
[a, b]The W-W distance between the neighboring W atoms at the corners and at the edges around the V_{WSe6}, respectively
[c]The energy gap for the half-metal

preferable than V_{Se2}. Hence, in the following study, only V_{Se-Se} is studied as the two Se atom vacancies. Additionally, the formation energies for the big size vacancies are higher, which may be generated via certain kind of structural engineering techniques [29–31].

We then studied the electronic properties of the defected monolayer WSe_2 with vacancies of V_{Se}, V_{Se-Se}, V_W, V_{W2}, V_{WSe3}, and V_{WSe6}. Figure 3 shows the electronic band structures of the six vacancy-doped monolayer WSe_2. As shown in Fig. 3a, V_{Se}-doped monolayer WSe_2 remains to be semiconducting, but there are obviously extra electronic states generated from the vacancy defect locating in the gap region. Consequently, the energy gap of V_{Se}-doped monolayer WSe_2 reduces to 1.18 eV compared with that of monolayer WSe_2. The electronic band structure of V_{Se-Se}-doped monolayer WSe_2 is similar with that of V_{Se}-doped monolayer WSe_2, and their energy gaps are close. V_W- and V_{WSe3}-doped monolayer WSe_2 shown in Fig. 3c and e also maintains the semiconducting feature but with much smaller energy gaps of 0.18 and 0.76 eV, respectively. Different from the above vacancy defects, the majority and the minority spin channels are distributed asymmetrically for the V_{W2}- and V_{WSe6}-doped monolayer WSe_2 as shown, in Fig. 3d and f. For the V_{W2}-doped monolayer WSe_2, the majority spin channels cross the Fermi level, while the minority spin channels maintain semiconducting with an energy gap of 0.19 eV, and its magnetic moment is 2.0 μ_B, while the V_{WSe6}-doped monolayer WSe_2 is magnetic semiconducting with a magnetic moment of 6.0 μ_B.

We also calculated the partial density of states (PDOS) for the six vacancy-doped monolayer WSe_2 to further study their electronic properties. Figure 4 shows that the impure electronic states of V_{Se}- and V_{Se-Se}-doped monolayer WSe_2 are mostly located in conduction band region, and they are mainly derived from the d orbital of W atoms near the vacancy, and little from p orbital of Se atoms around the vacancy. Differently, the impure electronic bands of V_W- and V_{WSe3}-doped monolayer WSe_2 are not only located in the conduction band region, but also being split in the valence band region. For V_W vacancy, the conduction bands near the Fermi level mainly come from the d (d_{xy}, $d_{x2}$and d_{z2}) orbitals of the W atoms around the vacancy, and the valence bands near the Fermi level are mainly from the p orbital of Se atoms around the vacancy. Compared with V_W-doped monolayer WSe_2, the impure electronic states of V_{WSe3}-doped monolayer WSe_2 are further away from the Fermi level. The conduction bands near the Fermi level are derived from both the Se $p_z$orbital and W d orbitals around the vacancy, while the valence bands near the Fermi level are mainly from the W d orbital around the vacancy. Additionally, W d orbital and the neighboring Se p orbital strongly interact, resulting in the hybridized states around the Fermi level. For the half-metallic V_{W2}-doped monolayer WSe_2, the conduction band cross of the Fermi level mainly comes from the Se $p_x$orbital, and the valence bands near the Fermi

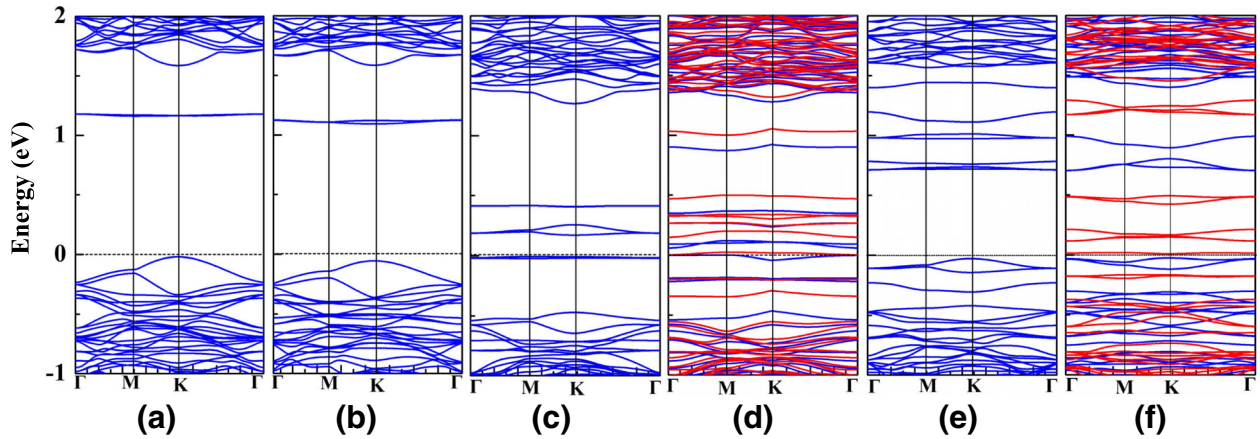

Fig. 3 The electronic band structures of monolayer WSe_2 with **a** V_{Se}, **b** V_{Se-Se}, **c** V_W, **d** V_{W2}, **e** V_{WSe3}, and **f** V_{WSe6} vacancies. Blue and red lines represent the majority and minority spin channels, respectively. Fermi level is set as 0 eV

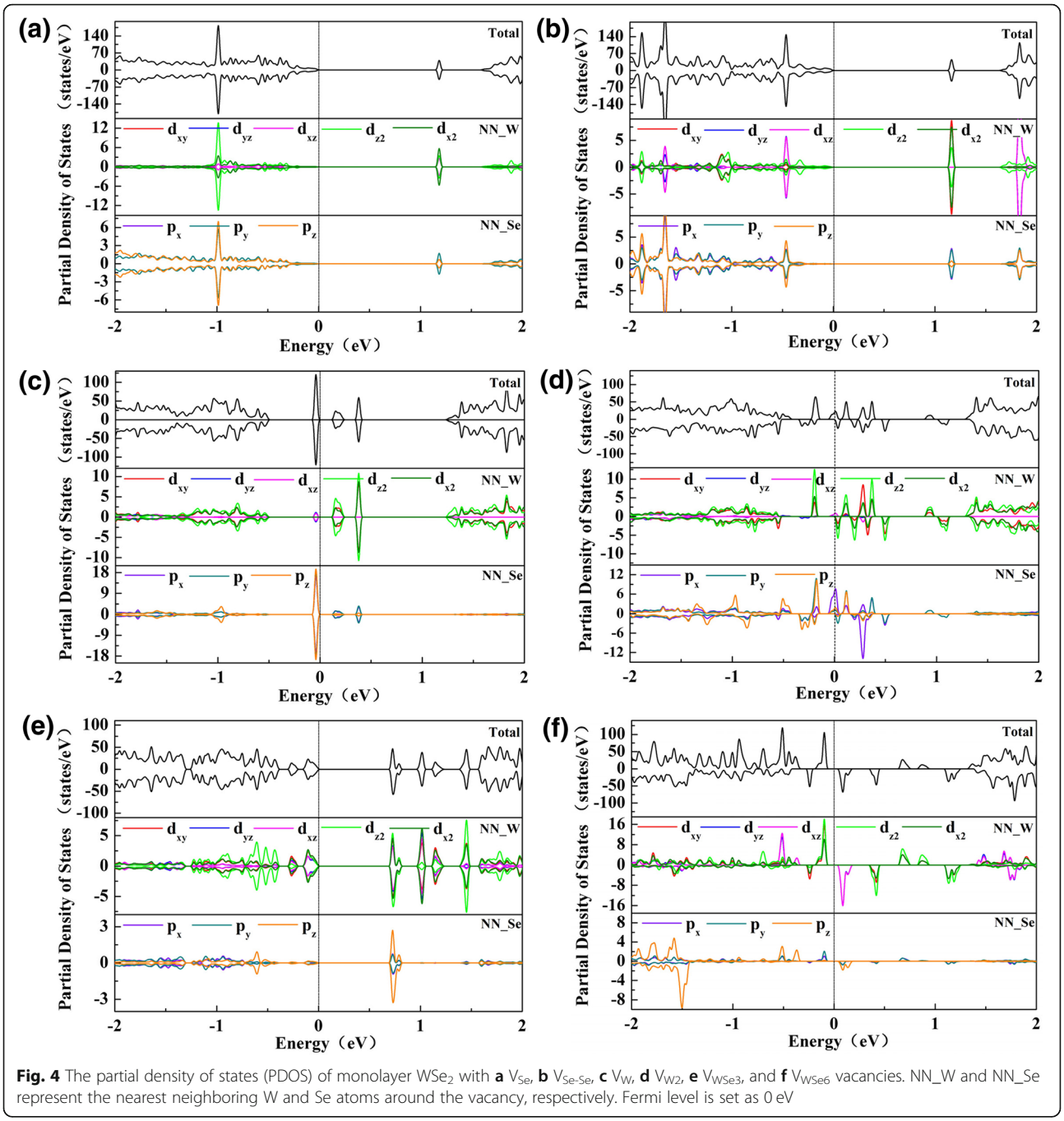

Fig. 4 The partial density of states (PDOS) of monolayer WSe_2 with **a** V_{Se}, **b** $V_{Se\text{-}Se}$, **c** V_W, **d** V_{W2}, **e** V_{WSe3}, and **f** V_{WSe6} vacancies. NN_W and NN_Se represent the nearest neighboring W and Se atoms around the vacancy, respectively. Fermi level is set as 0 eV

level are mainly derived from the W d (d_{x2} and d_{z2}) orbital. As for the magnetic semiconducting V_{WSe6}-doped monolayer WSe_2, the conduction bands and the valence bands near the Fermi level are both derived from the W d orbital near the vacancy.

The Electronic and Magnetic Properties of Monolayer WSe_2 with Vacancy Defect Under Tensile Strain

We further studied the electronic and magnetic properties of the vacancy-doped monolayer WSe_2 under the biaxial strain since the strain is an effective way to tune the electronic structures and magnetic moments of the 2D materials. We firstly studied the 1H-WSe_2 monolayer under the biaxial strain. Our calculation result shows that the biaxial strain ranging from 0 to 7% does not induce any magnetism into monolayer WSe_2, similar with monolayer MoS_2 [34, 36]. Additionally, monolayer WSe_2 still keeps the semiconducting nature with the energy gap decreasing to 0.5 eV at 7% strain, and the W-W bond length increases as the applied tensile strain increases.

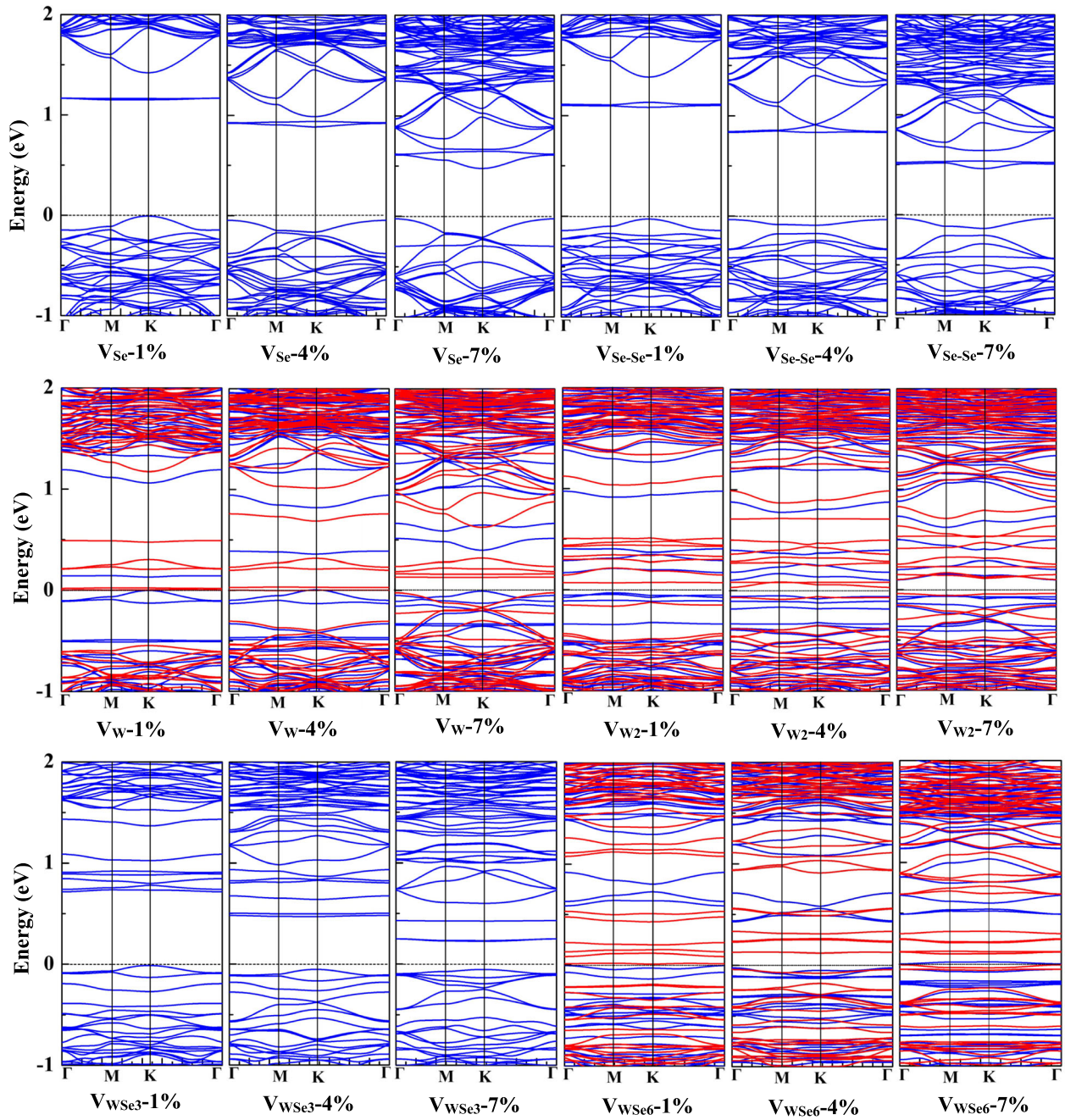

Fig. 5 The electronic band structures of monolayer WSe_2 with V_{Se}, $V_{Se\text{-}Se}$, V_W, V_{W2}, V_{WSe3}, and V_{WSe6} vacancies under 1%, 4%, and 7% tensile strain. Blue and red lines represent the majority and minority spin channels, respectively. Fermi level is set as 0 eV

Then, we studied the vacancy-doped monolayer WSe_2 under the tensile strain of 0~7%. Figure 5 shows the electronic band structures for V_{Se}-, $V_{Se\text{-}Se}$-, V_W-, V_{W2}-, V_{WSe3}-, and V_{WSe6}-doped monolayer WSe_2 under the biaxial strain of 1%, 4%, and 7%. Similar with the pristine WSe_2 monolayer, V_{Se}-, $V_{Se\text{-}Se}$-, and V_{WSe3}-doped monolayer WSe_2 all maintain the semiconducting feature under the biaxial strain of 0~7%, and the conduction band minima are getting closer to the Fermi level as the applied tensile strain increases. For the V_W-doped monolayer WSe_2 under the biaxial strain larger than 1%, the majority and minority spin channels distribute asymmetrically. Additionally, the V_{W2}- and V_{WSe6}-doped monolayer WSe_2 both show magnetic semiconducting feature under the strain of 1~7%. Though the V_{Se}-, $V_{Se\text{-}Se}$-, and V_{WSe3}-doped monolayer WSe_2 still keep the semiconducting feature under the biaxial strain of 0~7%, the biaxial strain effectively controls their energy gaps as shown in Fig. 6a. The

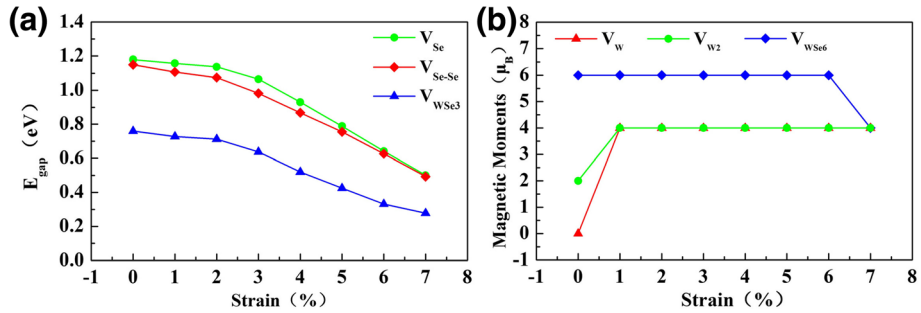

Fig. 6 **a** The energy gaps of monolayer WSe_2 with V_{Se}, $V_{Se\text{-}Se}$, and V_{WSe3} vacancies. **b** The magnetic moments of monolayer WSe_2 with V_W, V_{W2}, and V_{WSe6} vacancies under the tensile strain of 0~7%.

energy gaps of V_{Se}- and $V_{Se\text{-}Se}$-doped monolayer WSe_2 both decrease from 1.1 to 0.5 eV, while the energy gap of V_{WSe3}-doped monolayer WSe_2 is relatively smaller, which decreased from 0.76 to 0.3 eV. On the other hand, the energy gaps of V_W-, V_{W2}-, and V_{WSe6}-doped monolayer WSe_2 are less than 0.2 eV under the biaxial strain of 0~7%.

Under the biaxial strain of 0~7%, the V_{Se}-, $V_{Se\text{-}Se}$-, and V_{WSe3}-doped monolayer WSe_2 remain to be non-magnetic as shown in Fig. 5. In contrast, the non-magnetic V_W-doped monolayer WSe_2 become magnetic with the magnetic moment of 4 μ_B under the biaxial strain larger than 1%. The spin-resolved charge density shown in Fig. 7a indicates that the magnetic moment mainly arises from the W and Se atoms around the vacancies. As shown in Fig. 7b, the magnetic moment of V_{W2}-doped monolayer WSe_2 mainly comes from the Se atoms near the vacancy and little

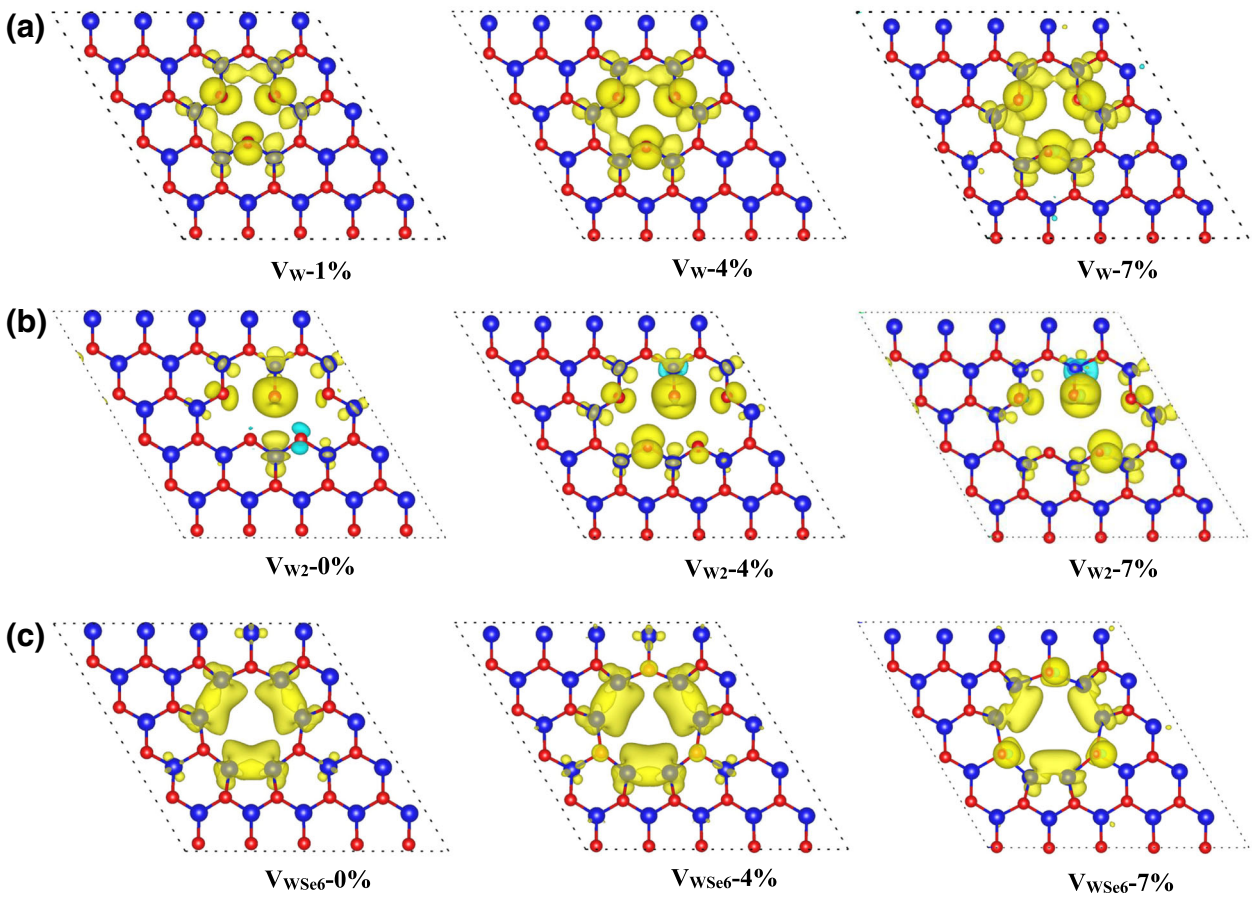

Fig. 7 Spin-resolved charge density of monolayer WSe_2 with **a** V_W, **b** V_{W2}, and **c** V_{WSe6} vacancies under the tensile strain of 0~7%. Yellow and cyan isosurfaces represent the positive and negative spin densities, respectively

from the W atoms around the vacancy. When the applied strain is larger than 1%, more Se atoms are spin-polarized, resulting in the larger magnetic moment of 4 μ_B. For V_{WSe6} vacancy defect, we can see that its magnetic moment remains to be 6 μ_B under the strain of 0~6% and then decreases to 4 μ_B at the strain of 7% as shown in Fig. 6b. Figure 7c demonstrates that its magnetic moments mainly arise from the six W atoms around V_{WSe6}. When the applied strain increases to 7%, the nearby Se atoms around the vacancy are more spin-polarized, but the local magnetic moments on the W atoms decrease. Correspondingly, the total magnetic moment of V_{WSe6}-doped WSe_2 decreases to 4 μ_B under 7% strain.

Conclusion

In summary, we studied several vacancy defects for monolayer WSe_2, including the single Se and W atom vacancies (V_{Se} and V_W), double Se and W atom vacancies ($V_{Se\text{-}Se}$ and V_{W2}), big vacancy of one W atom and the nearby three Se atoms on the same layer (V_{WSe3}), and vacancy of one W atom and the nearby three pairs of Se atoms (V_{WSe6}). The V_{Se}-, $V_{Se\text{-}Se}$-, V_W-, and V_{WSe3}-doped monolayer WSe_2 all keep the non-magnetic semiconducting feature as the perfect WSe_2 monolayer, but with smaller energy gaps due to the impure electronic states locating in the energy gap region, which are attributed from the W d and Se p orbital around the vacancies, while V_{W2} and V_{WSe6} vacancies induced magnetism into monolayer WSe_2 with magnetic moments of 2 and 6 μ_B, respectively. Particularly, monolayer WSe_2 with V_{W2} vacancy converts into half-metal from semiconducting. More importantly, our calculation results show that the external biaxial strain effectively tunes the magnetism and electronic properties of monolayer WSe_2.

Abbreviations

2D: Two-dimensional; CVD: Chemical vapor deposition method; DFT: The density functional theory; DOS: The density of states; HSE06: The Heyd–Scuseria–Ernzerh method; PAW: The projector augmented wave method; PBE: The Perdew–Burke–Ernzerhof method; PDOS: The partial density of states; TMDs: Transition metal dichalcogenides; VASP: Vienna Ab initio Simulation Package

Acknowledgements

Not applicable

Funding

This work was supported by the National key R&D Program of China (2018YFB0703800) and the National Natural Science Foundation of China (NNSFC) (21273172). This work was also supported by the 111 Project (B08040) and the Fundamental Research Funds for the Central Universities (3102015BJ(II)JGZ005, 3102015BJ023) in China.

Availability of Data and Materials

The datasets generated during and/or analyzed during the current study are available from the corresponding author on reasonable request.

Authors' Contributions

FXZ designed the study, performed the research, and drafted the original manuscript. DXY drafted the revised manuscript. YH and ZFL participated in part of the research. XLF supervise the research and revised the original and revised manuscript. All authors read and approved the final manuscript.

Competing Interests

The authors declare that they have no competing interests.

Publisher's Note

Received: 10 January 2019 Accepted: 6 May 2019
Published online: 04 June 2019

References

1. JY CAS, Karakaya M, Dandeliya S, Srivastava A, Lin Y, Rao AM, Podila R (2016) Defect-engineered graphene for high-energy- and high-power-density supercapacitor devices. Adv Mater 28:7185–7192
2. Geim AK, Novoselov KS (2007) The rise of graphene. Nat Mater 6(3):183–191
3. Fan XL, Wang SY, An YR, Lau WM (2016) Catalytic activity of MS_2 monolayer for electrochemical hydrogen evolution. J Phys Chem C 120:1623–1632
4. Choi W, Choudhary N, Han GH, Park J, Akinwande D, Lee YH (2017) Recent development of two-dimensional transition metal dichalcogenies and their applications. Materials Today 20(3):116–130
5. Fan XL, Yang Y, Xiao P, Lau WM (2014) Site-specific catalytic activity in exfoliated MoS_2 single-layer polytypes for hydrogen evolution: basal plane and edges. J Mater Chem A 2:20545–20551
6. Wang QH, Kalantar-Zadeh K, Kis A, Coleman JN, Strano MS (2012) Electronics and optoelectronics of two-dimensional transition metal dichalcogenides. Nature Nanotech 7(11):699–712
7. Fiori G, Bonaccorso F, Iannaccone G, Palacios T, Neumaire D, Seabaugh A, Banerjee SK, Colombo L (2014) Electronics based on two-dimensional materials. Nature Nanotech 9(10):768–779
8. Jariwala D, Sangwan VK, Lauhon LJ, Marks TJ, Hersam MC (2014) Emerging device applications for semiconducting two-dimensional transition metal dichalcogenides. ACS Nano 8(2):1102–1120
9. Yu QM, Shan WZ, Wang HM (2018) Theoretical design of sandwich two-dimensional structures for photocatalysts and nano-optoelectronic. J Mater Sci 53:8274–8284
10. Ataca C, Şahin H, Ciraci S (2012) Stable, single-layer MX_2 transition-metal oxides and dichalcogenides in a honeycomb-like structure. J Phys Chem C 116:8983–8999
11. Yun WS, Han SW, Hong SC, Kim IG, Lee JD (2012) Thickness and strain effects on electronic structures of transition metal dichalcogenides: 2H-MX_2 semiconductors (M = Mo, W; X = S, Se, Te). Phys Rev B 85:033305
12. Zhuang HL, Henning RG (2013) Computational search for single-layer transition-metal dichalcogenide photocatalysts. J Phys Chem C 117: 20440–20445
13. Fang H, Chuang S, Chang TC, Takei K, Takahashi T, Javey A (2012) High-performance single layered WSe_2 p-FETs with chemically doped contacts. Nano Lett 12(7):3788–3792
14. Ross JS, Klement P, Jones AM, Ghimire NJ, Yan J, Mandrus DG, Taniguchi T, Watanabe K, Kitamura K, Yao W, Cobden DH, Xu X (2014) Electrically tunable excitonic light-emitting diodes based on monolayer WSe_2 p-n junctions. Nature Nanotech 9(4):268–272
15. Baugher BWH, Churchill HOH, Yang YF, Jarillo-Herrero P (2014) Optoelectronic devices based on electrically tunable p-n diodes in a monolayer dichalcogenide. Nature Nanotach 9(4):262–267
16. Pospischil A, Furchi MM, Mueller T (2014) Solar-energy conversion and light emission in an atomic monolayer P-N diode. Nature Nanotech 9(4):257–261
17. Song HY, Lu JT (2018) Single-site point defects in semimetal WTe_2: A density functional theory study. AIP Advances 8(12):125323
18. Zhou W, Zou XL, Najmaei S, Liu Z, Shi YM, Kong J, Lou J, Ajayan PM, Yakobson BI, Idrobo JC (2013) Intrinsic structural defects in monolayer molybdenum disulfide. Nano Lett 13(6):2615-2622
19. Nair RR, Sepioni M, Tsai IL, Lehtinen O, Keinonen J, Krasheninnikov AV, Thomson T, Geim AK, Grigorieva IV (2012) Spin-half paramagnetism in graphene induced by point defects. Nature Phys 8(3):199–202
20. Yazyev OV (2010) Emergence of magnetism in graphene materials and nanostructures. Rep Prog Phys 73(5):56501–56516

21. Zhou YG, Yang P, Zu HY, Gao F, Zu XT (2013) Electronic structures and magnetic properties of MoS_2 nanostructures: atomic defects, nanoholes, nanodots and antidots. Phys Chem Chem Phys 15(25):10385–10394
22. Cao D, Cai MQ, Hu WY, Yu P, Huang HT (2011) Vacancy-induced magnetism in $BaTiO_3$(001) thin films based on density functional theory. Phys Chem Chem Phys 13(10):4738–4745
23. Cai MQ, Zhang YJ, Yin Z, Zhang MS (2005) First-principles study of structural and electronic properties of $BaTiO_3$(001) oxygen-vacancy surfaces. Phys Rev B 72(7):075406
24. Tongay S, Suh J, Ataca C, Fan W, Luce A, Kang JS, Liu J, Ko C, Raghunathanan R, Zhou J, Ogletree F, Li JB, Grossman JC, Wu JQ (2013) Defects activated photoluminescence in two-dimensional semiconductors: interplay between bound, charged, and free excitons. Sci Rep 3(6151):2657
25. Wu JX, Ma XL, Chen JZ, Jiang XW (2019) Defects coupling impacts on monolayer WSe_2 tunneling field-effect transistor. Appl Phys Express 12:034001
26. Zhao SD, Tao L, Miao P, Wang XJ, Liu ZG, Wang Y, Li BS, Sui Y, Wang Y (2018) Strong room-temperature emission from defect states in CVD-grown WSe_2 nanosheets. Nano Research 11(7):3922–3930
27. Zheng HL, Yang BS, Wang DD, Han RL, Du XB, Yan Y (2014) Tuning magnetism of monolayer MoS_2 by doping vacancy and applying strain. Appl Phys Lett 104(13):183
28. Zhou W, Zou XL, Najmaei S, Liu Z, Shi YM, Kong J, Lou J, Ajayan PM, Yakobson BI, Idrobo JC (2013) Intrinsic structural defects in monolayer molybdenum disulfide. Nano Lett 13(6):2615-2622
29. Komsa HP, Kotakoski J, Kurasch S, Lehtinen O, Kaiser U, Krasheninnikov AV (2012) Two-dimensional transition metal dichalcogenides under electron irradiation: defect production and doping. Phys Rev Lett 109(3):035503
30. Krasheninnikov AV, Nordlund K (2010) Ion and electron irradiation-induced effects in nanostructured materials. J Appl Phys 107(7):071301
31. Xie LM, Jiao LY, Dai HJ (2010) Selective etching of graphene edges by hydrogen plasma. J Am Chem Soc 132(42):14751–14753
32. Wang X, Dai H (2010) Etching and narrowing of graphene from the edges. Nature Chem 2(8):661–665
33. Pan H, Zhang YW (2012) Tuning the electronic and magnetic properties of MoS_2 nanoribbons by strain engineering. J Phys Chem C 116(21):11752–11757
34. Shi HL, Pan H, Zhang YW, Yakobson BI (2013) Strong ferromagnetism in hydrogenated monolayer MoS_2 tuned by strain. Phys Rev B 88(20):5326–5333
35. Bertolazzi S, Brivio J, Kis A (2011) Stretching and breaking of ultrathin MoS_2. Acs Nano 5(12):9703–9709
36. Tao P, Guo HH, Yang T, Zhang ZD (2014) Strain-induced magnetism in MoS_2 monolayer with defects. J Appl Phys 115(5):054305
37. Cooper RC, Lee C, Marianetti CA, Wei XD, Hone J, Kysar JW (2013) Nonlinear elastic behavior of two-dimensional molybdenum disulfide. Phys Rev B 88(3):035423
38. Yang SX, Wang C, Sahin H, Chen H, Li Y, Li SS, Suslu A, Peeters FM, Liu Q, Li JB, Tongay S (2015) Tuning the optical, magnetic, and electrical properties of $ReSe_2$ by nanoscale strain engineering. Nano Lett 15:1660–1666
39. Yang Y, Fan XL, Pan R, Guo WJ (2016) First-principles investigations of transition-metal doped bilayer WS_2. Phys. Chem. Chem. Phys 18:10152
40. Kresse G, Furthmuller J (1996) Efficiency of ab-initio total energy calculations for metals and semiconductors using a plane-wave basis set. Com Mater Sci 6(1):15–50
41. Cristol S, Paul JF, Payen E, Bougeard D, Clemendot S, Hutschka F (2000) Theoretical study of the MoS_2 (100) surface: a chemical potential analysis of sulfur and hydrogen coverage. J Phys Chem B 104(47):11220–11229
42. Perdew JP, Burke K, Ernzerhof M (1996) Generalized gradient approximation made simple. Phys Rev Lett 77(18):3865–3868
43. Kresse G, Joubert D (1999) From ultrasoft pseudopotentials to the projector augmented-wave method. Phys Rev B 59(3):1758–1775
44. Hobbs D, Kresse G, Hafner J (2000) Fully unconstrained noncollinear magnetism within the projector augmented-wave method. Phys Rev B 62(17):11556–11570
45. Monkhorst HJ, Pack JD (1976) Special points for Brillouinzone integrations. Phys Rev B 13(12):5188
46. Heyd J, Scuseria GE, Ernzerhof M (2003) Hybrid functionals based on a screened Coulomb potential. J Chem Phys 118(18):8207–8215